J Mater Sci

Electronic materials

Adhesion of reactive silver inks on indium tin oxide

Avinash Mamidanna[1], April Jeffries[2], Mariana Bertoni[3], and Owen Hildreth[1,*]

[1] *Department of Mechanical Engineering, Colorado School of Mines, Golden, CO 80401, USA*
[2] *School for Engineering of Matter, Transport and Energy, Arizona State University, Tempe, AZ 85287, USA*
[3] *School of Electrical, Computer and Energy Engineering, Arizona State University, Tempe, AZ 85287, USA*

Received: 1 August 2018
Accepted: 9 October 2018

ABSTRACT

Many emerging photovoltaic technologies, such as silicon heterojunction (SHJ) cells and perovskites, are temperature sensitive and are not compatible with the high sintering temperatures required for commercial screen-printed metallization pastes. Newer, low-temperature reactive silver inks exhibit good electrical conductivity and are compatible with temperature-sensitive substrates. However, preliminary investigations showed that the adhesion and reliability of these metallizations could vary dramatically with ink composition. This work evaluates the adhesion performance of printed reactive inks on indium tin oxide-coated SHJ cells to show that puckering phenomena originating from the porous nature of the printed reactive inks are responsible for lowering the as-printed adhesion strength. Adhesion performance was qualitatively determined using 180° peel test followed by optical imaging to quantify the amount of adhesive failure. Post-print scanning electron microscopy was used to observe the surface morphology. Diluting the reactive ink to reduce silver ion concentration decreased the observed puckering phenomenon and improved adhesion performance. This new understanding enables a more systematic design of reactive inks for novel photovoltaic applications.

Introduction

Photovoltaic solar cells require electrical contacts on both the front and back surfaces to facilitate current collection. Frontside electrodes typically consist of metallic grids, which are designed to minimize power losses due to resistive losses and shadowing [1]. Often frontside grids have high-aspect ratio fingers less than 60 μm wide and greater than 30 μm high to provide high current-carrying cross-sectional area while minimizing shadowing effects [2]. Frontside electrodes of most commercial photovoltaic cells are manufactured using screen-printed silver pastes [3, 4]. These pastes consist of Ag particles in a mixture of SiO_2 particles, solvents, binders, and other resistive materials that modify the rheology of the paste and improve adhesion [2]. A heat treatment step is required after screen-printing to drive off the organic additives, to thermally sinter the silver particles together for improved electrical conductivity,

Address correspondence to E-mail: ohildreth@mines.edu

https://doi.org/10.1007/s10853-018-3017-6

Published online: 16 October 2018

and to establish a reliable electrical contact with the silicon substrate [5–8].

Many emerging photovoltaic architectures show potential for high efficiency, but contain layers that are not compatible with traditional silver paste metallizations. For example, silicon heterojunction (SHJ) cells contain hydrogenated amorphous Si passivation layers that degrade above 200 °C [9]. Therefore, low-cure-temperature silver pastes must be used. However, these have relatively high media resistivities and use significantly more silver per solar cell—about 200 mg Ag/cell compared to 100 mg Ag/cell for high-cure-temperature Ag pastes. Additionally, SHJ cells are topped with a transparent conducting oxide made of indium tin oxide (ITO) to improve lateral transport of current to the front grid. Our previous work with reactive silver inks (RSI) has demonstrated that RSI are a promising new metallization method for photovoltaic cells compatible to thermally sensitive substrates [10]. While these results were encouraging, internal testing showed that the adhesion between the reactive silver ink metallizations and the underlying substrate varied with small changes in ink composition and substrate temperature during printing. Given that delamination at the adhesion layer can be a primary failure mechanism in photovoltaic cells [11, 12], this work aims to elucidate the underlying mechanism for as-printed delamination at the Ag/ITO interface and demonstrate preliminary reactive inks with good adhesion.

In this study, 180° peel test experiments were performed to characterize the adhesion strength of drop-on-demand (DOD) printed silver metallization lines on ITO. A narrowed parameter space investigation of ink concentration and number of layers is carried out with a goal to differentiate "good" adhesion from "poor" adhesion, where "good" adhesion is defined as metallization layers showing less than 5% area loss in a 180° tape peel test as measured from top-down optical microscopy. A low-temperature, self-reducing, amine-stabilized reactive silver ink was used as the basis of this study [13]. Previous work has shown that the porosity of this ink can be varied from 50% up to 90% by simply adjusting substrate temperature, solvent heat of vaporization, and silver ion concentration [14]. By varying the ink composition and number of layers, this work will show that adhesion strength varies with the porosity of the printed RSI. For example, inks that produce highly porous films result in decreasing adhesion strength with increasing number of layers. This is attributed to an increase in puckering and delamination at the silver/ITO interface as solvent percolates through the porous network, becomes trapped within the silver film, and leads to voids as solvent evaporation increases internal pressure. Inks that produce dense films showed reduced levels of puckering, and while the adhesion strength initially decreases, it then recovers as the number of layers increases. Overall, this work shows suppressing of the puckering phenomena to deposit silver lines with good adhesion to ITO-coated substrates using DOD-printed RSI. Thus, this work enables the formation of low-resistance, low-cost, low-temperature metallization of photovoltaic cells.

Experimental section

Ag reactive ink synthesis and chemistry

A low-temperature, self-reducing silver diamine reactive ink solution was used as the basis for the RSI used in this study [13]. All solid chemicals were used as received, and liquid chemicals were filtered through a nylon filter with a manufacturer-stated pore size of 450 nm.

Two gram of silver acetate ($C_2H_3AgO_2$, anhydrous, Alfa Aesar, 99%) was dissolved in 5.00 mL ammonium hydroxide (NH_4OH, VWR, 28–30 wt%, ACS Grade) followed by 0.4 mL formic acid (HCOOH, Sigma-Aldrich, Anhydrous, > 96%) added dropwise. The ink was allowed to sit for 12 h in the dark under ambient conditions and then filtered through a 450-nm nylon/polypropylene filter. The ink was then stored at ~ 4 °C until use. The referenced RSI recipe [13] used 2,3-butanediol as a humectant to stabilize the droplets and make printing easier. However, previous studies have shown that the low vapor pressure of the 2,3-butanediol increases porosity and decreases electrical conductivity [14]. Instead, the base silver ink described above was diluted with either 1:1 or 1:10 by volume with ethanol (silver ink/ethanol). This replacement somewhat decreases ink stability, requiring better control over applied pressure and a narrower DOD printing parameter window. However, using ethanol has been shown to reduce porosity and improve the as-printed electrical resistivity of the RSI films [14]. The ink solution was filtered one last time immediately prior to printing.

The chemical reactions for silver formation are based on a modified Tollens' process. The proposed overall reaction along with the intermediate steps for this process is as follows [13]:

$$AgCH_3CO_2 + NH_4OH + CH_2O_2 \rightarrow [Ag(NH_3)_2]^+[C_2H_3O_2]^- \rightarrow Ag \quad (1)$$

The overall reaction shows the key components in the reactive ink solution. Initially, the silver acetate (metal salt) dissolves in the ammonium hydroxide (complexing agent) and formic acid (reducing agent). These three together form a stable silver diamine complex, that is self-reducing to metallic silver under either the application of heat or decrease in ammonia concentration via evaporation. Equations 2 and 3 show the proposed intermediate steps in which the silver acetate and dilute ammonium hydroxide precipitate a silver oxide intermediate that dissolves in aqueous ammonia to form a silver diamine complex.

$$2AgCH_3CO_2 + 2NH_4OH \rightarrow Ag_2O + 2NH_4CH_3CO_2 + H_2O \quad (2)$$

$$Ag_2O + 4NH_3 + 2NH_4CH_3CO_2 + H_2O \rightarrow 2Ag(NH_3)_2CH_3CO_2 + 2NH_4OH \quad (3)$$

When formic acid is added to the solution, any unprotected silver is reduced to form particles that are removed by sedimentation (~ 31% by weight). The remaining formic acid (40% by weight) neutralizes the ammonium hydroxide by protonating the hydroxide to water and forming ammonium formate (NH_4CO_2). The final solution that contains diamine silver (I) cations and acetate and formate anions constitutes the reactive ink. As the ink dries, the ammonia evaporates, allowing the silver cations to be reduced by the formate anions as well as acetic acid produced in solution from uncomplexed silver that was previously reduced.

$$2Ag(NH_3)_2CH_3CO_2 + 2NH_4CO_2 \rightarrow 2Ag + 5NH_3 + 2CH_3CO_2H + CO_2 + H_2O \quad (4)$$

$$2Ag(NH_3)_2CH_3CO_2 + 2NH_4CO_2 \rightarrow Ag + AgCH_3CO_2H + 5NH_3 + CH_3CO_2H + CO_2 + H_2O \quad (5)$$

This combination of formate and acetate ions along with acetic acid leads to reduction to silver and silver acetate particles when dried at room temperature. However, at higher temperatures, elemental silver is the only phase that remains due to fast evaporation of ammonia ligands and other low boiling point reactants. For a more detailed explanation of all the intermediate steps, refer Supporting Information of Walker and Lewis' work [13].

Device fabrication and peel testing

ITO-coated substrates were fabricated by coating 2 cm × 4 cm silicon substrates with 80 nm of ITO deposited using DC magnetron sputtering. An O_2 plasma surface treatment was conducted immediately prior to RSI printing to improve the wetting of the silver inks on the ITO surface. This improves the continuity of the silver during DOD printing. O_2 plasma treatments were performed in a Venus 25 Plasma Etch system at 60 W for 5 s with 0.01 L/min of O_2 and 0.005 L/min Ar held at 0.2 torr.

Contact angle measurements were collected from reactive silver ink pipetted on ITO/Si substrates before and after plasma treatment to confirm that the substrate was hydrophilic. An in-house goniometer was constructed from Dino-Lite AM3111T handheld digital microscope and a Litepanels Sola ENG backlight source. DinoXcope software was used to capture the contact angle images, and ImageJ was then used to estimate the contact angles of the droplets from the captured images. Prior to plasma treatment, the contact angle of undiluted RSI on ITO was measured at 67°. After plasma treatment, the RSI droplets were found to completely spread on the ITO surface with contact angles less than 10° (the smallest angle that could be measured using this setup).

All printing was done using a MicroFab Jetlab II with precision stage and a digital pressure controller. During printing, the ITO-coated substrates were held at 66 °C as measured by thermocouple in contact with the top of the substrate. The camera and strobe built into the Jetlab II were used to observe drop formation, droplet diameter, and droplet velocity. Printing was done using a 60-μm orifice diameter nozzle (MicroFab, MJ-ATP-01-60-DLC). The printing parameters shown in Table S1 in Supporting Information were optimized to minimize satellite droplets and maximize droplet stability.

Printing and peel tests

Preliminary peel tests were conducted with the 1:1 RSI ink printed with 3, 7, and 15 layers on the ITO/Si

substrate. Each of the 3-, 7-, and 15-layer samples consisted of three printed Ag lines, 40 mm in length and spaced 3 mm apart (Fig. 1). The three Ag lines within a sample set were named L_1, L_2, and L_3 corresponding to the top, center, and bottom lines, respectively.

Next, to test the effects of droplet diameter on adhesion, the printing parameters were varied to produce 28 μm and 35 μm droplet diameters, as listed in Table S1 in Supporting Information. 1, 3, 5, 7, 9, 11, 13, and 15 layers were printed for the 1:1—Ag/ethanol ink, while up to 75 layers were printed for the 1:10 ink. 75 layers were chosen to deposit a comparable mass of silver per unit width as in a 15-layer line of the 1:1 sample (see Supporting Information Fig. S1). Peel tests were conducted on the samples, and failure analysis and average line widths were quantified from the stitched optical images using Adobe Photoshop CS and ImageJ software (see Supporting Information Fig. S2).

180° peel tests were conducted using a general-purpose masking tape (Duck™; see Sect. 4 of Supporting Information for tape down-selection process) with a pull speed of 1 cm/min, and a 5 N Instron 2530 low-profile load cell with an accuracy of equal to or better than 0.25% of the indicated force was used to obtain load versus extension plots. A masking tape was applied to the sample using a 150 g metallic roller. Preliminary tests were performed to ensure that the weight of the roller did not affect the morphology of the printed metal contacts. See Fig. S3–S5 in Supporting Information for the complete explanation of the peel test setup, tape selection process, and tape application validation process. Pre-peel and post-peel tested images of the printed Ag lines were captured using an MX61A Olympus microscope and stitched together using Stream Motion software (version: 1.6) to represent the entire printed line. Additionally, pre-peel and post-peel tested SEM images were collected using an Amray 1910 Field Emission SEM. 3D profilometry maps 1 mm wide and 4 mm long were collected using a Dektak Stylus profilometer with a tip radius of 2 μm.

High-speed video of droplets

A glass slide was cleaned prior to droplet deposition and placed on a substrate held at 66 °C. Five microliter of a 1:1 RSI was then pipetted onto the glass slide, and the droplet evolution was captured using a Navitar UX100 high-speed camera along with a 6 × zoom body with 3 mm fine focus. This was repeated for multiple layers to simulate the effect of printing multilayered silver contacts on ITO.

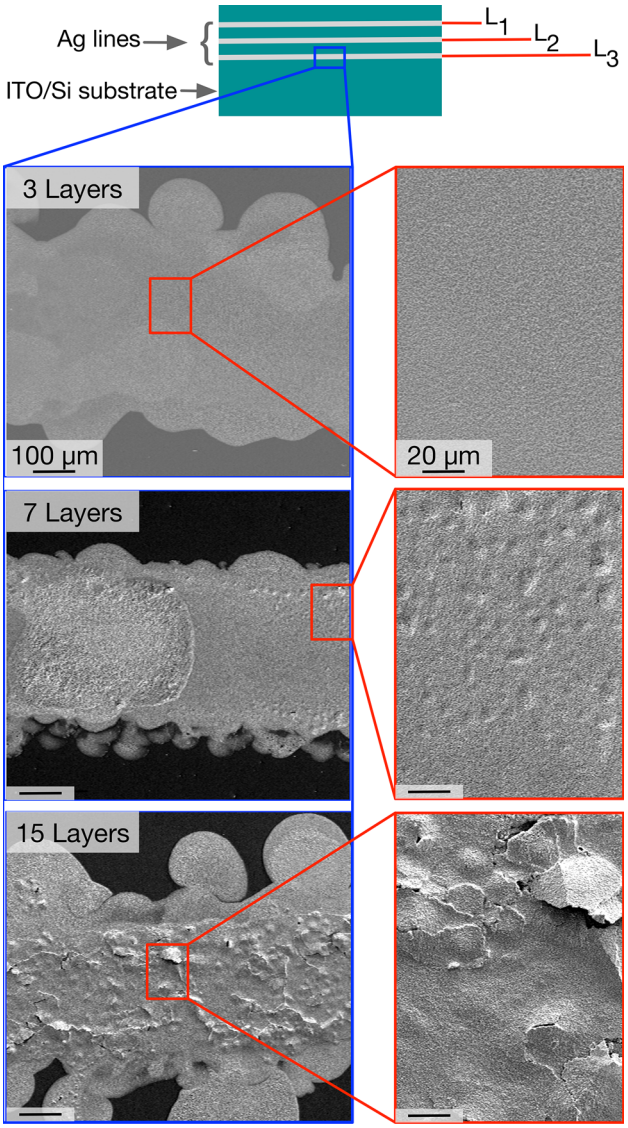

Figure 1 Schematic of silver lines printed on ITO/Si followed by top-down SEM micrograph of a 3, 7, and 15-layer samples printed using Ag/ethanol—1:1 ink shown from top to bottom. Zoomed-in regions of the printed lines are shown on the right for clearer view of puckering effects. The puckering effect becomes more prominent as the number of layers increases. Scale bars for the images on the left are 100 μm and 20 μm for the images on the right.

Results and discussion

Preliminary peel tests were conducted on silver lines printed on ITO/Si. Figure 1 shows a schematic of the silver lines on ITO/Si before peel testing followed by top-down SEM micrographs of the printed silver lines from three different samples printed with 3, 7, and 15 layers of silver, respectively.

The lines marked L_1, L_2, and L_3 from the schematic correspond to the top, center, and bottom lines of each printed sample set. The SEM image of the 3-layer sample shows a relatively uniform printed line. For the 7-layer sample, small divots and rough abnormalities are observed in the silver line morphology, and in the 15-layer sample, these effects were significantly more pronounced with numerous regions within the printed line appearing to pucker and flake off from the substrate. From these preliminary results, it appears that puckering increases with increasing number of layers. This puckering implies that the silver is delaminating from the ITO substrate and the adhesion strength is expected to decrease. Thus, as the number of layers increases to reduce the resistance of the printed silver line, the adhesion strength will decrease. This tradeoff presents a challenge since ideal front-grid metallization requires both good adhesion strength and high-aspect ratio fingers for minimizing resistive and power losses.

180° peel tests were used to verify that increasing puckering leads to decreases in adhesion strength. Qualitative and quantitative analyses of the 3-, 7-, and 15-layer samples post-peel testing are presented in top-down SEM images in Fig. 2a. Figure 2b shows the load versus extension curves for the three samples. While the observed adhesive failure within the printed silver line of the 3-layer sample was minimal at less than 5%, approximately 25 and 70% area loss was observed in the 7-layer and 15-layer samples, respectively. The vertical red lines labeled L_1, L_2, and L_3 indicate the locations of the three silver lines within each sample set. Peaks in load were observed as the tape passed over the three Ag lines in the 3- and 7-layer samples during peel testing. The peaks occur due to higher adhesion force between the tape and Ag, compared to the tape and ITO (see Supporting Information Fig. S6). Reduction in the magnitude of the peak force for the 7-layer samples indicates decreasing mean adhesion strength and, in this case, increase in as-printed delamination and puckering. For the 15-layer sample, the peaks are replaced with dips, indicating that the net adhesion strength within the silver film is less than the adhesion between the tape and the ITO. Overall, the extensive puckering seen in the 15-layer sample prior to peel test resulted in lower adhesive strength of the printed silver lines.

It is important to understand how printing parameters influence puckering and as-printed delamination. Since the parameter space for DOD printing and reactive inks is large, this study limited itself to using the silver diamine reactive ink (see Experimental Methods) with the best characteristics for solar cell front-grid metallization as determined in earlier studies; The silver diamine reactive ink used in this study was printed at 66 °C using the parameters optimized for low porosity and media resistivity [14]. With these parameters kept constant, the droplet diameter, ink dilution (1:1 and 1:10—silver reactive ink/ethanol by volume), and number of layers were varied. This variation in number of layers within the optimal parameter space allows for additional optimization of both adhesion strength and line resistance. Ink dilution impacts contact angle, silver ion concentration, and porosity. The 1:10 diluted inks found to produce films with the lowest porosity for that study (~ 55%) [14]. Furthermore, droplet diameter impacts the amount of silver ions in each droplet along with the time it takes to evaporate each droplet [15].

Preliminary tests suggested that droplet diameter impacted adhesion for the 1:1 inks. First, to systematically test this, silver lines were printed with the Ag/ethanol—1:1 ink dilution using two different droplet sizes, 28 μm and 35 μm. These diameters represent the range of droplet diameters that were reproducible from the same nozzle through adjusting printing parameters. Since different droplet diameters deposit different amounts of silver/droplet and also deposit different line widths, the data were normalized by the mass of silver deposited per unit width (see Supporting Information for the original data). The percentage of adhesive failure area in Fig. 3 was measured using top-down optical images of the samples. Figure 3a, b plots the mass of Ag per unit width (μg/μm) versus failure area and peak-to-valley roughness (R_z). The top-down optical images on the left show the representative images for the 28 μm (blue border) and 35 μm (red border) droplets.

The failure area within the lines after peel testing increases with increasing droplet diameter and the

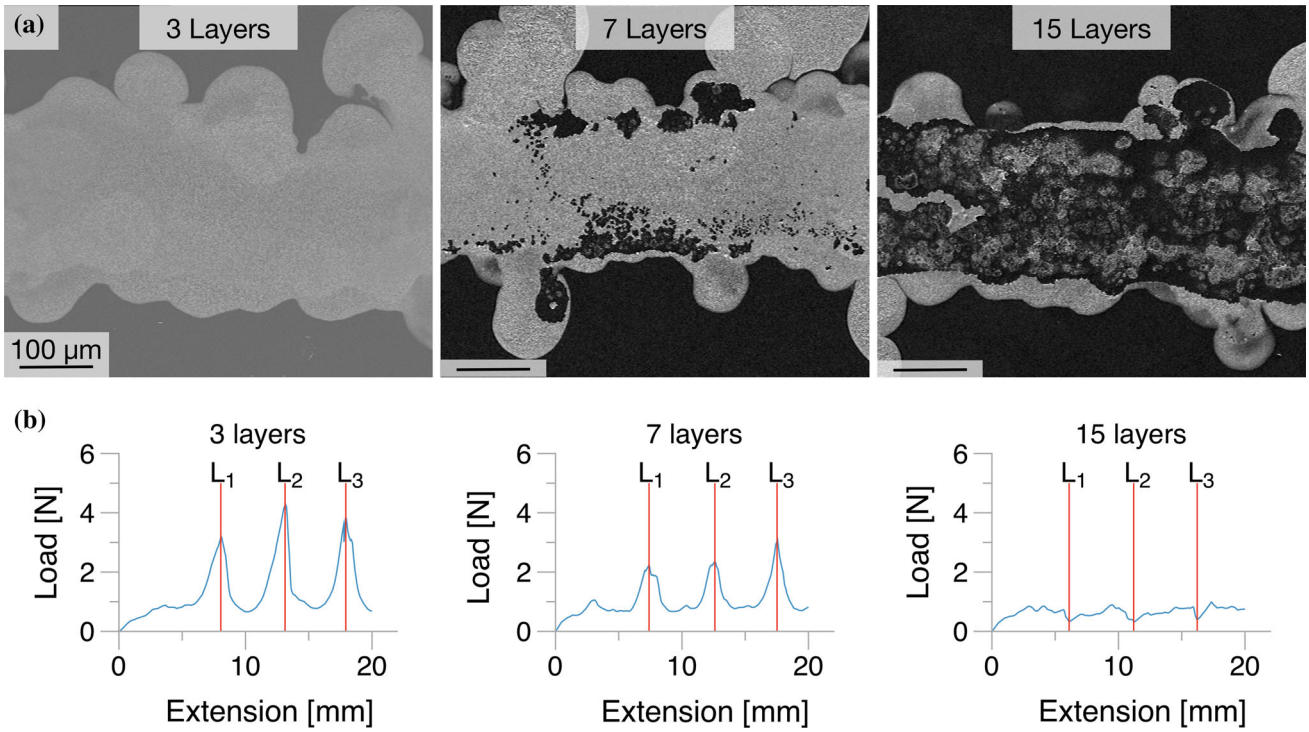

Figure 2 **a** SEM top-down micrographs of 3, 7, and 15-layer samples after peel testing using masking tape. The 3-layer sample does not exhibit any visible adhesive failure. The 7-layer sample shows a few regions of adhesive failure, and the 15-layer sample exhibits extensive adhesive failure; **b** Load versus extension plots for the 3, 7, and 15-layer silver lines are shown. The magnitude of load peaks is slightly lesser for the 7-layer sample as we noticed an onset of adhesive failure, and for the 15-layer samples, a dip in the load curve is observed indicating maximum failure within the printed silver line. All scale bars are 100 µm.

number of layers as seen in Fig. 3a. Note that the amount of failure is greater in the larger droplet samples reaching 55% failure compared to the 15% for the smaller droplet samples. This implies that the failure increases with number of layers or increasing silver content within each printed line. The peak-to-valley roughness of the printed samples was also observed to increase with increasing puckering and increased failure area as seen in Fig. 3b. R_z is greater for larger droplet samples reaching a maximum of about 40 µm, and R_z for the smaller droplet samples is lesser in comparison and peaks at about 25 µm. This further solidifies the conclusion that as silver content per line increases, the puckering effect also increases leading to higher failure area during peel testing. The increasing failure area with increasing number of layers can clearly be visualized from the optical top-down images for both the samples as shown on the right of Fig. 3 where the underlying silicon substrate (light blue) is exposed within the silver line area.

In the next study, the 1:10 dilution ink was used for printing to test adhesive failure from peel testing in denser lines. Silver lines were printed with the Ag/ethanol—1:10 ink dilution with a droplet diameter of 35 µm. Figure 4 shows a similar layout to Fig. 3 and shows plots of Ag/width versus failure area and R_z on the left and optical top-down images of the lines after peel testing on the right for this specific ink dilution and droplet diameter. (For full-size optical images of all sample sets, refer Supporting Information Fig. S7–S9.)

The overall adhesive failure for the 1:10 sample is lesser than the 1:1 samples and peaks at about 15% failure area at about 0.015 µg/µm of silver. After increasing the silver content beyond about 0.015 µg/µm, the adhesive failure starts to decrease. Also, R_z for this sample set is much lower compared to the 1:1 samples and peaks at about 10 µm, indicating reduced puckering or printing-induced delamination within the sample. For a more comprehensive view of all three sample sets, refer Supporting Information Fig. S10–S11.

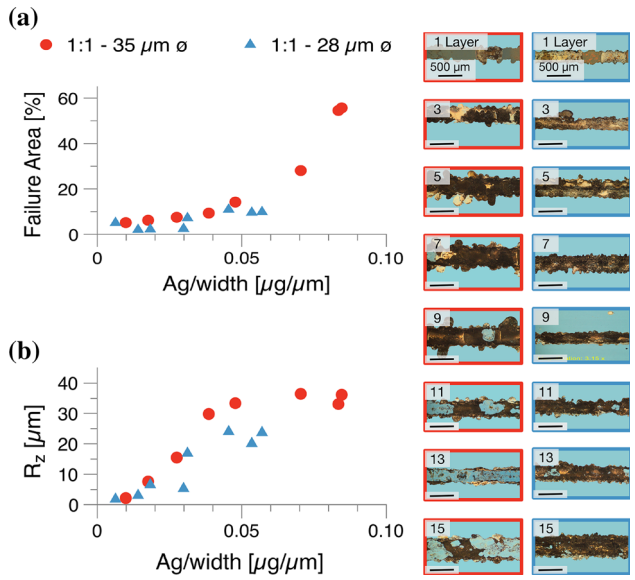

Figure 3 **a** Plots for Ag/width versus failure area using Ag/ethanol—1:1 ink with 28 μm and 35 μm droplet size (blue—28 μm droplet, and red—35 μm droplet samples); the failure area increases as Ag/width (e.g., number of layers) increases in both cases. Failure area is greater for the 35 μm droplet sample indicating more adhesive failure; **b** plots for Ag/width versus R_z shows that peak-to-valley roughness also increases as Ag/width increases for both droplet sizes. R_z for the larger droplet reaches a higher maximum indicating more printing-induced puckering. On the right are optical top-down images of a small portion of the printed lines for both droplet sizes showing adhesive failure.

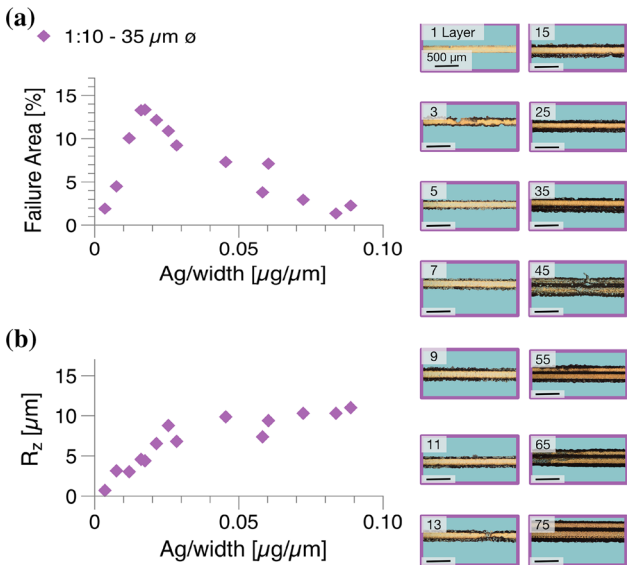

Figure 4 aPlots for Ag/width versus failure area using Ag/ethanol—1:10 ink with 35 μm droplet size; the failure area increases as Ag/width (e.g., number of layers) increases until 11 layers are printed and then starts decreasing; **b** plots for Ag/width versus R_z show that peak-to-valley roughness also increases slightly as Ag/width increases, although the magnitude of R_z is much lower compared to the 1:1 samples. This indicates that the magnitude of printing-induced delamination is smaller for the 1:10 samples. On the right are optical top-down images of a small portion of the printed lines showing adhesive failure. The dark regions are due to scattering where the silver film is very rough.

The origin of the puckering phenomena is still under investigation; however, it is possible to speculate contributing mechanisms. The sequence in Fig. 5 illustrates a likely puckering mechanism. The left and center columns schematically illustrate the sequence of events and what the cross section of the film would look like. The right column shows top-down images of 1:1 RSI taken with a high-speed camera. It is known that the films produced with these reactive inks are highly porous [14] and that the solvents used in the inks will likely percolate through any open-cell networks. As a result, an existing silver film is likely to be porous (Fig. 5a). As additional layers are printed, the ink will quickly percolate through the porous film (Fig. 5b). The RSI used in this study is stabilized by an excess of ammonia and will quickly reduce to form solid silver at the liquid/vapor interface near the top of the droplet (where the ammonia evaporates the quickest). Depending on the size and shape of the pores and the thickness of the porous layer, substrate temperature, and ammonia evaporation rate, either one of two things is likely to occur: (1) the pores are large enough or the film is thin enough that the reaction proceeds without closing the pores and the solvent is able to escape; or (2) the pores are thin enough and film thick enough that the pores near the top surface of the silver film close off before the percolated solvent can completely escape. In the first case, the adhesion will not degrade. In the second case, puckering will be observed as the trapped solvent vaporizes and, unable to escape, it causes the film to locally break apart (Fig. 5c and d). Each subsequent layer would increase the amount of puckering until the film completely degrades leading to more printing-induced delamination (Fig. 5e).

For the 1:1 samples, the pores are small with respect to the film thickness. As a result, the ink from subsequent layers seeps through the pores. Since silver self-reduces as the ammonia concentration decreases, the pores at the liquid/vapor interface quickly seal up where the ammonia rapidly evaporates from the surface. This sealing phenomenon

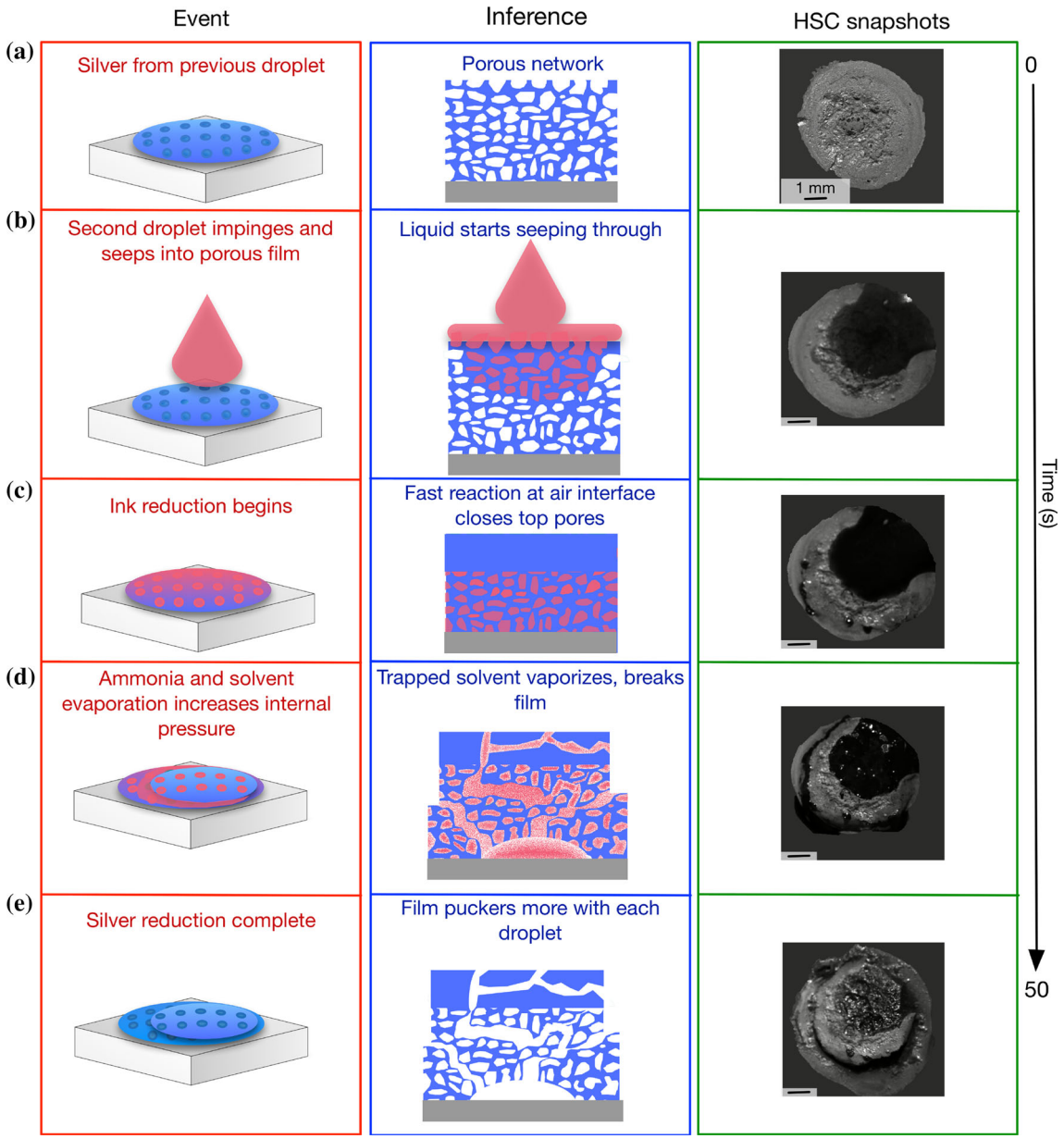

Figure 5 Schematic of droplet evolution of a second RSI droplet on a porous silver structure leading to puckering. The schematics in the left column indicate the various stages of a multilayered evolution. The center column shows 2D cross-sectional schematics of the different stages, and the image on the right is the top-down high-speed camera video snapshots corresponding to each stage.

traps the remaining solvents, which increases internal pressures as these solvents heat up and then vaporize. This internal pressure can be relieved if either the silver film breaks apart or if the silver film delaminates from the substrate. While the exact ratio between the two failure mechanisms is unknown at this time, it is clear from Figs. 3 and 4 that substrate temperature and ink composition impact the which failure mechanism dominates.

Previous studies by Lefky et al. [14] showed that the porosity of the silver diamine (I) ink varies with substrate temperature, solvent selection, and dilution. In general, these studies showed that dilute inks produced less porous films than concentrated inks and that inks diluted in solvents with high vapor pressure also produced less porous films. In this work, we chose ink dilutions (1:1 and 1:10) to match those of Lefky et al. so that the impact of dilution, its corresponding porosity, and the resulting adhesion

strength could be loosely correlated. As shown by Lefky et al., samples printed with the 1:10 inks are inherently denser and pore sizes smaller than the samples printed with the 1:1. We propose that the adhesion strength of the films printed with this particular silver diamine reactive ink decreases with increasing porosity and that denser films increase adhesion strength by reducing the amount of solvent trapped within the evaporating film. The decrease in adhesion strength with increasing number of layers is attributed to the repeated straining of the substrate/film interface as the ink from each additional layer seeps through the film to the substrate/film interface and evaporates.

The initial increase in failure area of the 1:10 ink followed by a decrease in failure area (see Fig. 4a) is still under investigation. We suspect that the lower porosity and thinner film produced by the 1:10 ink allow the film to "recover" from the early damage caused by trapped solvents. Specifically, any breaks in the initial few layers could be filled in by later layers in a manner that doesn't trap solvent and lead to delamination of the film. While the exact mechanism for delamination is still under investigation, these results do show that silver films with good adhesion to ITO-coated substrates can be deposited at temperatures conducive to SHJ and other temperature-sensitive applications.

Conclusion

In this study, the impact of solvent dilution and the number of layers on the adhesion between DOD-printed RSI inks and ITO substrates were investigated. Two different dilutions of the reactive ink (RSI/ethanol—1:1 with 28 μm and 35 μm droplets, and RSI/ethanol—1:10 with 35 μm droplets) and varying number of layers were used to understand the effect of the concentration and amount of silver on a printed contact. Inks with higher silver concentration resulted in more puckering and lower adhesion. Diluting the ink 1:10 by volume with ethanol showed significant improvements in adhesion strength, with under 5% area failure during the adhesive peel test (compared to 51% in the higher concentration RSI ink). Most importantly, we show that adhesion of reactive ink metallizations can be significantly improved while still forming high-aspect-ratio silver lines. Through printing of diluted inks with small droplet diameters and multiple-layer thickness, high-adhesion-strength, low-resistance front-grid metallizations can be formed from DOD-printed reactive inks. These results highlight the complex interactions between reaction kinetics, mass transport, and heat transfer on the external device outputs such as adhesion and series resistance. The high adhesion strength exhibited by the 1:10 RSI recipe can pave the way for reliable low-temperature metallization on SHJ solar cells at reduced costs.

Acknowledgements

This work was supported by the National Science Foundation under contract agreement IIP-1602135 and CMMI-1635548. Any opinions, findings, and conclusions or recommendations expressed in this material are those of the author(s) and do not necessarily reflect those of the National Science Foundation.

Compliance with ethical standards

Conflict of interest The authors declare that there is no conflict of interest.

Electronic supplementary material: The online version of this article (https://doi.org/10.1007/s10853-018-3017-6) contains supplementary material, which is available to authorized users.

References

[1] Teng KF, Vest RW (2004) Application of ink jet technology on photovoltaic metallization. IEEE Electron Device Lett 9:1–2

[2] Ebong A, Chen N (2015) Metallization of crystalline silicon solar cells: a review. In: 2012 9th International conference on high capacity optical networks and enabling technologies (HONET). IEEE, pp 102–109

[3] Hermans JP, Papet P, Oacheco K, et al. (2014) Advanced metallization concepts by inkjetprinting. pp 1–6. https://doi.org/10.4229/eupvsec20142014-2co.2.3

[4] Shaheen SE, Radspinner R, Peyghambarian N, Jabbour GE (2001) Fabrication of bulk heterojunction plastic solar cells by screen printing. Appl Phys Lett 79:2996–2998. https://doi.org/10.1063/1.1413501

[5] Teng KF, Vest RW (2004) Metallization of solar cells with ink jet printing and silver metallo-organic inks. IEEE Trans Compon Hybrids Manuf Technol 11:1–7

[6] Li ZG, Liang L, Ionkin AS et al (2011) Microstructural comparison of silicon solar cells' front-side Ag contact and the evolution of current conduction mechanisms. J Appl Phys 110:074304–074309. https://doi.org/10.1063/1.3642956

[7] Li ZG, Liang L, Cheng LK (2009) Electron microscopy study of front-side Ag contact in crystalline Si solar cells. J Appl Phys 105:066102–066104. https://doi.org/10.1063/1.3086663

[8] Rane SB, Khanna PK, Seth T et al (2003) Firing and processing effects on microstructure of fritted silver thick film electrode materials for solar cells. Mater Chem Phys 82:237–245. https://doi.org/10.1016/S0254-0584(03)00236-0

[9] De Wolf S, Descoeudres A, Holman ZC, Ballif C (2012) High-efficiency silicon heterojunction solar cells—a review. Green 2:1–19. https://doi.org/10.1515/green-2011-0018

[10] Jeffries AM, Mamidanna A, Ding L, Hildreth O, Bertoni MI (2016) Low-temperature drop-on-demand reactive silver inks for solar cell front-grid metallization. IEEE J Photovolt 7:37–43. https://doi.org/10.1109/JPHOTOV.2016.2621351

[11] Paretkar D, Glassmaker NJ, Mikeska KR, Blackman G, Jagota A (2016) Adhesion of screen-printed silver metallization to crystalline silicon solar cells. IEEE J Photovolt 6:1141–1151. https://doi.org/10.1109/JPHOTOV.2016.2583792

[12] Ndiaye A, Charki A, Kobi A et al (2013) Degradations of silicon photovoltaic modules: a literature review. Sol Energy 96:140–151. https://doi.org/10.1016/j.solener.2013.07.005

[13] Walker SB, Lewis JA (2012) Reactive silver inks for patterning high-conductivity features at mild temperatures. J Am Chem Soc 134:1419–1421. https://doi.org/10.1021/ja209267c

[14] Lefky C, Mamidanna A, Huang Y, Hildreth O (2016) Impact of solvent selection and temperature on porosity and resistance of printed self-reducing silver inks. Phys Status Solidi A 213:2751–2758. https://doi.org/10.1002/pssa.201600150

[15] Talbot EL, Berson A, Brown PS, Bain CD (2012) Evaporation of picoliter droplets on surfaces with a range of wettabilities and thermal conductivities. Phys Rev E 85:061604–061606. https://doi.org/10.1103/PhysRevE.85.061604